Journal of Power Sources 196 (2011) 2717–2724

Contents lists available at ScienceDirect

Journal of Power Sources

journal homepage: www.elsevier.com/locate/jpowsour

Effect of dynamic operation on chemical degradation of a polymer electrolyte membrane fuel cell

Minjae Jung*, Keith A. Williams

Department of Mechanical Engineering, 290 Hardaway Hall, Box 870276, The University of Alabama, Tuscaloosa, AL 35487-0276, United States

ARTICLE INFO

Article history:
Received 27 October 2010
Accepted 28 October 2010
Available online 3 December 2010

Keywords:
PEM fuel cells
Dynamic operation
Fluoride release
Chemical degradation

ABSTRACT

Dynamic operation is known as one of the factors for accelerating chemical degradation of the polymer electrolyte membrane in a polymer electrolyte membrane fuel cell (PEMFC). However, little effort has been made dealing with the quantification of the degradation process. In this investigation, cyclic current operation is carried out on a fuel cell system, and the frequency effect of cyclic operation on chemical degradation is investigated. The dynamic behavior of a fuel cell system is analyzed first with the modified Randles model, where the charge double layer is modeled by three components; a charge transfer resistance (R_{ct}), and two RC cells for the Warburg impedance. After calculating each parameter value through exponential curve fitting, the dynamic behaviors of the three components are simulated using MATLAB Simulink®. Fluoride release as a function of the frequency of cyclic operation is evaluated by measuring the concentration of fluoride ion in effluent from a fuel cell exhaust. The frequency effect on chemical degradation is explained by comparing the simulated results and the fluoride release results. Two possible reasons for the accelerated degradation at cyclic operation are also suggested.

1. Introduction

The proton exchange membrane fuel cell (PEMFC) has been considered a candidate for future vehicular and stationary applications and has the advantages of high current density, high fuel efficiency, and low temperature operation, although technical problems remain. One of the main issues limiting the application of a PEMFC is membrane degradation which is mainly caused by three factors, mechanical, thermal and chemical degradation [1]. If it is assumed that sufficient temperature control of a fuel cell system can be realized, such that thermal degradation may be neglected, mechanical degradation is thought to be the main cause of early failure [1], and chemical degradation usually results in a significant drop in the performance before the failure [2].

A number of previous research efforts have shown that the chemical degradation is mainly attributed to chemical attack of highly reactive oxygen radicals formed in the fuel cell [1–3]. Although the mechanisms describing how these radicals form and attack the membrane are still unclear, it is now generally considered that the formation of hydrogen peroxide (H_2O_2) plays an important role in the chemical attack. The formation of hydrogen peroxide and reactive oxygen radicals is a multi-step process including oxygen gas crossover and is shown below in Fig. 1 [1,3]. Hydrogen fluoride (HF) is a direct product of the radical attack on the membrane. As such, the rate of chemical degradation can be evaluated by measuring the fluoride content of the effluent from the fuel cell exhaust [4]. As fluoride release continues, the membrane thickness decreases, which is called 'membrane thinning' [4], and eventually, leads to the generation of pin-holes which further degrade the system by allowing hydrogen to pass directly through the membrane and "burn" with oxygen on the platinum catalyst at the cathode side of the fuel cell.

There are several factors that may accelerate the chemical degradation. Severe degradation due to operation with low humidification and operation with an open circuit voltage, but no net current has been reported and investigated by multiple researchers [5–7]. A great deal of research effort has been focused on determining the relation between those factors and membrane degradation, but those relations have not yet been fully clarified. Liu and Case reported that dynamic operation also accelerated the chemical degradation by showing that there is about a one order difference in fluoride release between cyclic operation and constant operation of a PEMFC [8]. However, there has been little further research on the effect of dynamic operation on chemical degradation.

The goal of this research is an examination of the influence of dynamic operation on accelerated degradation of a fuel cell system. The PEMFC used in this research was a Ballard Nexa 1.2 kW fuel cell system, and dynamic operation was realized using a transistor switch controlled by an ON and OFF pulse signal as shown in Fig. 2. In this figure, R_{PL} is a parasitic load resistor composed of the

* Corresponding author. Tel.: +82 10 5607 1130; fax: +82 31 8056 5518.
E-mail address: aidenian06@gmail.com (M. Jung).

0378-7753/$ – see front matter © 2010 Elsevier B.V. All rights reserved.
doi:10.1016/j.jpowsour.2010.10.105

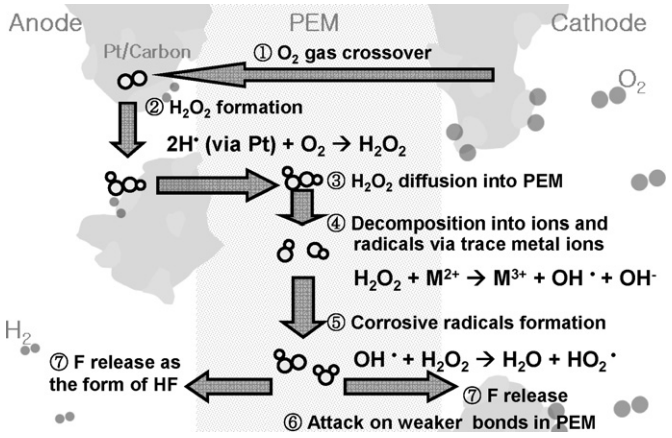

Fig. 1. Mechanism of chemical degradation of a PEM membrane.

fuel cell control system and balance of plant (cooling fan, compressor, solenoid valves), and R_L is an exterior load resistor. Different operation conditions were modified by changing the frequency of the pulse signal. For the sake of this work, the dynamic behavior of PEMFC was first investigated. The Nexa system was modeled by a simplified Randles model for which parameters were evaluated using curve-fits and the dynamic behavior of the fuel cell system as the pulse input was varied was simulated using MATLAB software. The rate of chemical degradation during operation with different frequencies was determined by measuring the concentration of fluoride ions released in the water drained from the fuel cell system using a fluoride ion selective electrode. The fluoride is usually released from both the anode and the cathode, and the release rate is determined using the effluent collected from both sides [2]. However, the product water of the Nexa system is just from the cathode side because the system has a dead end structure where the anode outlet is blocked. Accumulation of nitrogen and water vapor in the hydrogen stream gradually increases with time, so the anode is purged to flush out inert constituents periodically [9]. It is believed that the fluoride released from the anode would be exhausted with the anode gas when it is purged, and there is also fluoride exhausted in the form of a gas from the cathode. Without consideration of the amount of these fluoride gases, it is very difficult to determine absolute amount of the fluoride released from fuel cells. In this research, the value of the fluoride emission rate measured using the ion selective electrode does not mean the absolute value of the total HF emission from the fuel cell system. The rate of chemical degradation is compared by comparing the fluoride release rate of the tests at different operating frequencies. Finally, the frequency effects on both simulated dynamic behavior and chemical degradation were compared and their close relationship was shown.

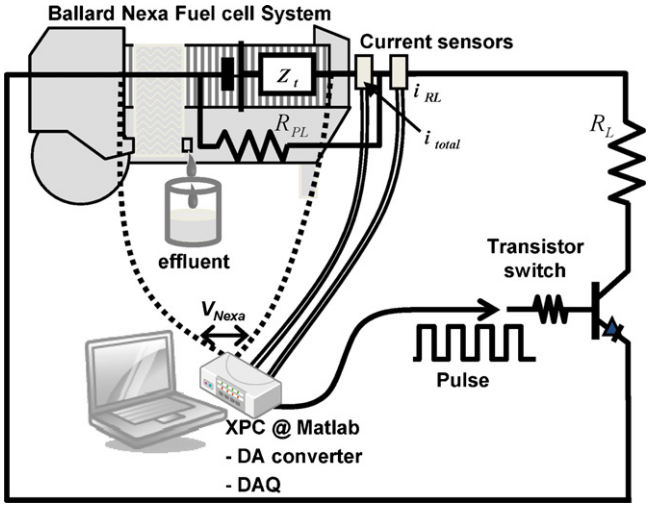

Fig. 2. Experimental setup for dynamic operation of the Ballard Nexa fuel cell system. Z_t is a total impedance of the Nexa system.

2. Experimental setup

The schematic diagram of the Ballard Nexa fuel cell system is seen in Fig. 2. To dissipate the fuel cell power, a 0.77 Ω resistor with a 1 kW power dissipation rating was implemented by parallel connection of a 1 Ω and three 10 Ω resistors (FSE-1000, Huntington Electric Inc.). The duty ratio of the pulse signal was fixed at 15% and 50% in which the 15% duty cycle means 15% externally loaded and 85% parasitic load only, and the pulse frequency was varied from 0.0005 Hz to 1 kHz. A transistor switch was constructed to perform the step loading and unloading of the system using a high-current complementary transistor (MJ11032) and a diode. The switch signal and data acquisition were realized using a standard DAQ card controlled using the MathWorks software package XPC. Fluoride release rates during operation of the fuel cell system were evaluated by collecting effluent from the exhaust and measuring the fluoride ion concentration using a fluoride ion selective electrode (Hach, Model No. 51928; a concentration range for the measurement is from 0.01 mg L^{-1} F to saturated solutions, and a slope change for the concentration is -58 ± 3 mV per decade [10]). Preparation of a standard solution and calibration were performed by the direct measurement method as described in its manual [10]. The fluoride release rate was calculated by measuring the fluoride concentration and condensation rate of the cathode product water.

3. Results

3.1. Modeling and simulation

The voltage and current changes during cyclic operation are shown in Fig. 3. The stack current cannot be completely turned off because there is always a parasitic load current (i_{RPL}), so the cyclic operation condition in this research has no open circuit condition. Furthermore, under the assumption of well-controlled humidification of the Nexa system, the only accelerating degradation factor in this experiment is assumed to be the dynamic operation.

The equivalent circuit in Fig. 4 is used to model the fuel cell system as described in a previous effort [11] in which the charge double layer is modeled by three pairs of resistors and capacitors

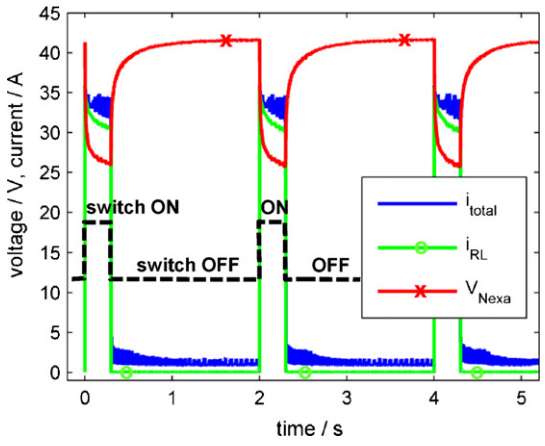

Fig. 3. Voltage and current changes during cyclic operation.

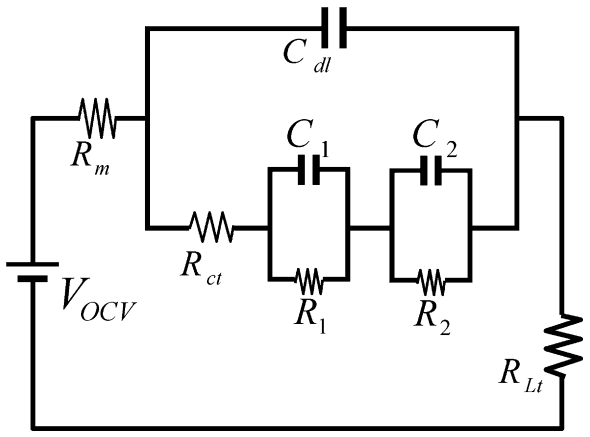

Fig. 4. An equivalent circuit of the Nexa system modeled by the simplified Randles model. V_{OCV}, R_m, R_{Lt} are open circuit voltage, membrane resistance, and total load resistance including R_{PL} and R_S (switch resistance).

components: a charge transfer resistance (R_{ct}), and two *RC* cells. By assuming that the oxygen reduction reaction rate in the cathode is much lower than the hydrogen oxidation reaction rate and that the charge double layer is represented by a pure capacitance in parallel with the charge transfer resistance, the equivalent circuit of a fuel cell can be simplified using just one Randles model [11]. The Warburg impedance of the Randles circuit can usually be approximated by pairs of resistances and capacitances (*RC* cells) in series, and two RC cells are used for the Warburg impedance in our research [11]. The first *RC* cell (R_1 and C_1) is used to model the time delay related to water diffusion inside the membrane, and the second *RC* cell (R_2 and C_2) is used to model gas diffusion in the gas diffusion layer. Values for each of the parameters were calculated through exponential curve fitting. The fitting results using three exponential curves are shown in Fig. 5. The voltage transient occurring during a load implementation is termed a "down curve" (switch ON) and the voltage transient occurring during a load removal is termed an "up curve" (switch OFF). If the modified Randles model in Fig. 4 is employed, the down and up curves can be represented by three exponential curves. Therefore, six independent equations for evaluating six parameters (R_{ct}, C_{dl}, R_1, C_1, R_2, and C_2) can be set up using three exponential curves [11]. In fitting the up curve, the modified voltage curve for fitting is a negative exponential curve converging to zero with time. The fitted curves, three exponential curves, and their sum are also negative, but they are expressed as positive values by adding the stabilized value of the off state voltage as shown in Fig. 5(b). The curve fitting and calculation are performed by the software package MATLAB, and the results show that the parameter values calculated from the down curves are not same as those of the up curves. The noticeable reason for this difference can be found in compressor operation of the Nexa system. The fitting range for the down curve is performed for the data collected prior to the acceleration of the compressor, but the range for the up curve is at the already accelerated compressor speed [11].

Since the down curve and up curves are different from each other, the parameter values calculated from these two curves are also different. Each parameter value calculated from the experimental data of 50% duty ratio and 0.2 Hz under the assumption of neglecting the current to the parasitic load (i_{RPL}) was summarized

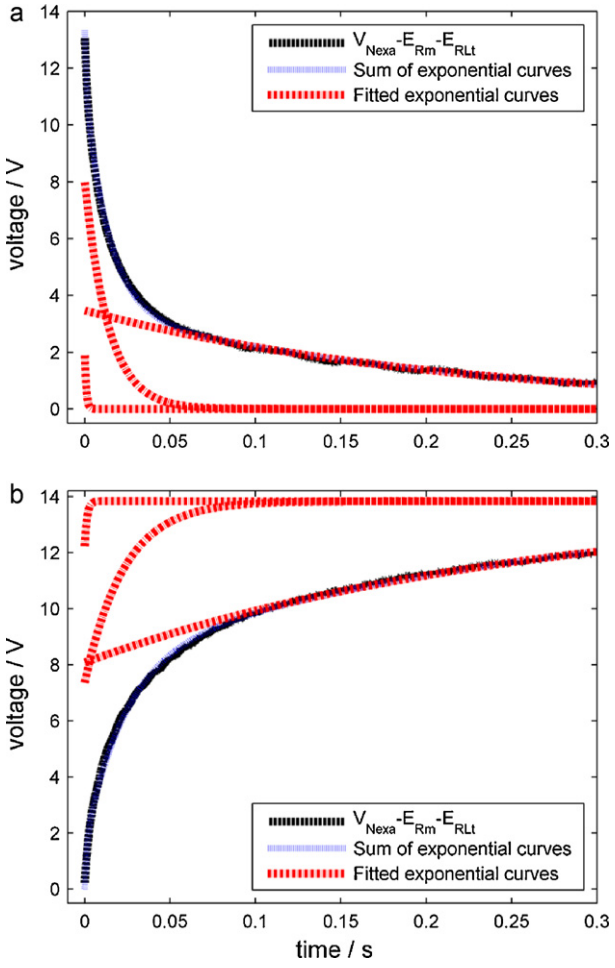

Fig. 5. Curve fitting using three exponential curves of (a) down curve and (b) up curve.

in Table 1. The simulation was conducted twice for the down and up curve differently using MATLAB Simulink® as shown in Fig. 6, and the results were plotted in Fig. 7.

Due to the difference of parameter values between down and up curves, it is difficult to reproduce the continuous voltage response to the high frequency pulse input especially in cases with asymmetric duty ratios such as 15%. The simulation was performed at 50% of duty ratio for checking the possibility to reproduce the voltage profile at high frequency using the parameter values calculated from low frequency data of 0.2 Hz. In Fig. 8, it can be seen that the simulation results compare well with experimental results of various frequencies. For the purpose of the continuous plot, all starting points of up curves were brought into the end points of down curves. The current to the parasitic load slightly changes in terms of the frequency, so R_{Lt} should be modified for simulating high frequency response. R_{Lt} at each frequency in Fig. 8 was calculated using data between 4 s and 5 s of the experimental curve where the voltage is locally stabilized.

In cyclic operation of the Nexa system, a period mismatch is shown between the input signal and compressor operation. At low frequencies, the compressor speed is low when the switch is off

Table 1
Parameter values of Randles model.

	V_{OCV} (V)	R_m (Ω)	C_{dl} (F)	R_{ct} (Ω)	R_1 (Ω)	C_1 (F)	R_2 (Ω)	C_2 (F)	R_{Lt} (Ω)
Down curve	41.82	0.0908	0.0168	0.0718	0.145	1.668	0.213	0.0631	0.825
Up curve	41.82	0.0866	0.0213	0.0807	0.177	1.442	0.187	0.101	0.842

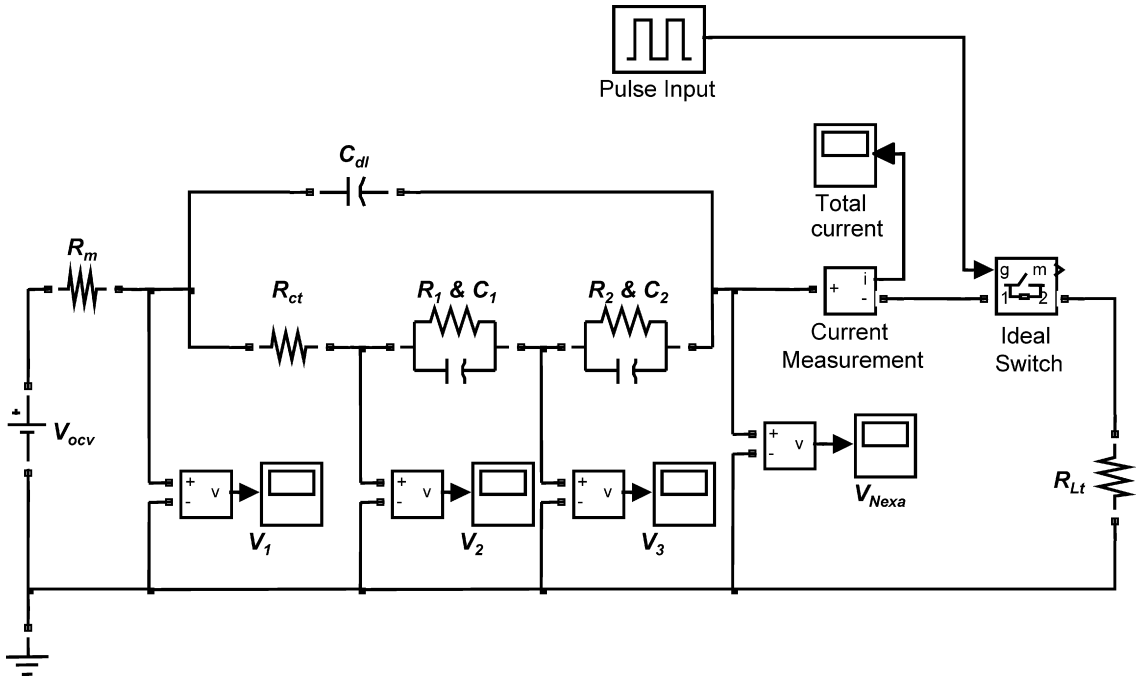

Fig. 6. Simulink model of the Ballard Nexa fuel cell system.

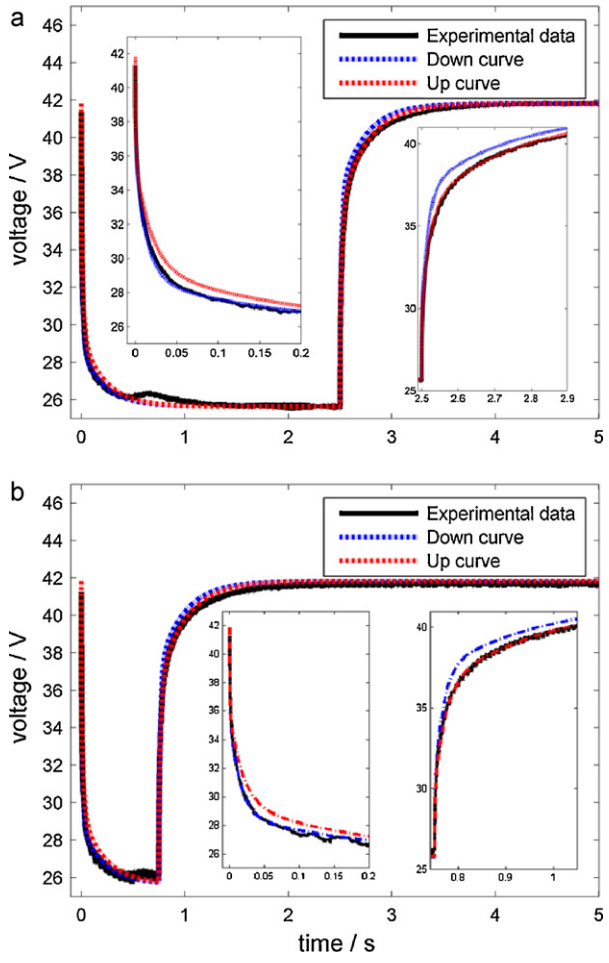

Fig. 7. Voltage response reproduced by Simulink® using the calculated parameters (a) duty ratio is 50% and (b) duty ratio is 15%.

(open), and the rate is high when the switch is on (closed), so the compressor speed generally follows the input signal. However, with increasing frequencies, the compressor speed does not track the input signal as well. This is believed to be due to the inertia of the compressor; as the switch is closed and opened more frequently, the compressor cannot speed up or slow down quickly enough to track the varying load. At the frequency range between about 1 Hz and 20 Hz, the period of the compressor operation keeps bouncing back and forth with much longer frequencies than the input frequency. Eventually, with higher input frequencies, the compressor speed becomes relatively constant. The longer frequency of the compressor could explain the discrepancy between experimental and simulated data in Fig. 8(a) in which the voltage drop of the experiment is getting bigger due to the continuous operation of the compressor of which the magnitude gradually increases for a while. The results at higher frequencies in Fig. 8(b)–(d) show discrepancies during early stage of the operation, but the simulated results matched well with the experimental data except these initial differences.

3.2. Analysis of dynamic behavior

The experimental data can show only the total voltage drop, but the simulation shown in Fig. 6 can be used to estimate the voltage drop caused by each *RC* component. The simulation results of each component as the frequency of the pulse input changes are plotted in Fig. 9. In the result for the charge transfer resistance (R_{ct}), the full voltage oscillation responding to the input signal occurs up to about 20 Hz, and the oscillation amplitude decreases as the frequency increases. The 0.1 Hz and 0.2 Hz traces are not visible on the plots (Fig. 9(a) and (b)) because they are underneath the 1 Hz trace. Due to the small value of C_{dl} (0.01–0.02 F) and R_{ct} (0.07–0.08 Ω), there are still oscillations, even at the relatively high frequency of 100 Hz. Similar results were obtained for other two *RC* cells, but the frequency ranges at which oscillation amplitudes are attenuated are dependent on *RC* values. Although different values for the down and up curves were used, the dynamic behavior of each *RC* cells are similar between both curves. The results are summarized in Table 2.

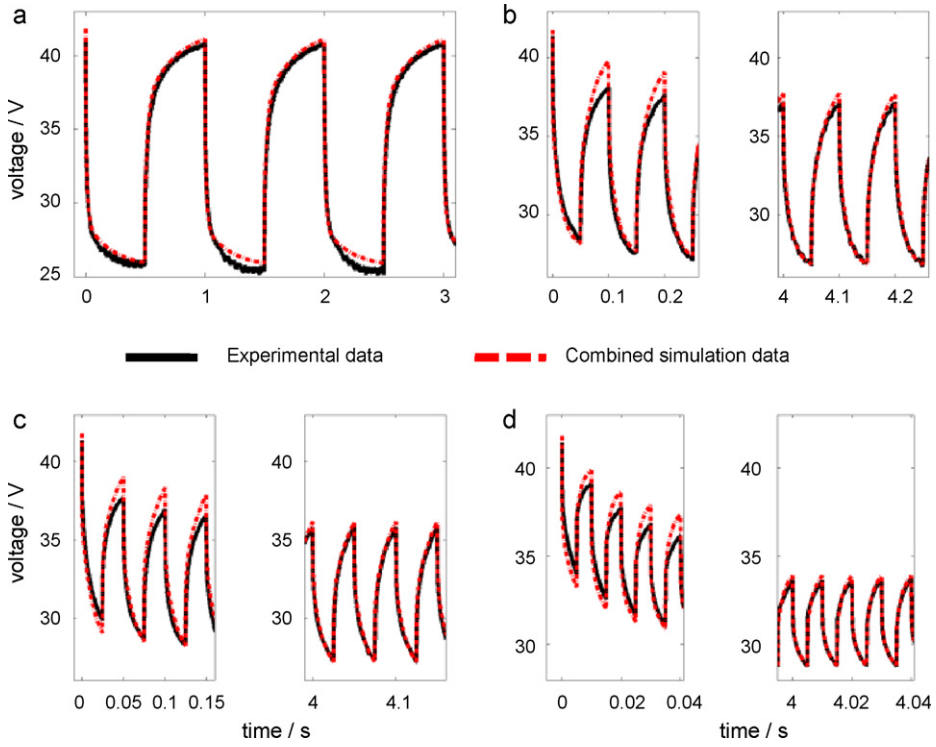

Fig. 8. Voltage Merged curve of down and up curves simulated at (a) 1 Hz, (b) 10 Hz, (c) 20 Hz, and (d) 100 Hz. Modified RLt at each frequency is 0.825, 0.805, 0.775, 0.775 Ω for the down curve, and 0.842, 0.705, 0.692, 0.662 Ω for the up curve respectively.

3.3. Chemical degradation during dynamic operation

As described previously, chemical degradation continues during non-operation of the Ballard Nexa system. Cessation of operation can make the chemical degradation all the worse. Therefore, it is important to ensure how long the fuel cell system has been without operation before performing experiments that will be used to assess the variation of membrane degradation as a function of the input signal. To remove the effect of potential chemical degradation due to the fuel cell system not being used for periods of time, constant-current aging was performed on the Nexa system before each such experiment. For example, since the fuel cell system had not been operated for about 1 month before the first experiment, constant current aging was conducted for 4.5 h for the first experiment. For subsequent experiments, constant-current operation was performed for 2.5 h to mitigate potential degradation due to the systems' being inactive overnight. More operating details are provided below in Table 3. For each frequency, dynamic operation of the fuel cell was performed for a specific duration. At fixed times during operation, effluent samples were taken and tested for the concentration of HF. For all inputs except at 0.1 Hz, test durations were 7 h. For the 0.1 Hz input, an additional 4.5 h of testing were performed, to provide insight into any time-dependence of the fluoride emissions over that long time period. No such dependences were found. For all other tests, the duty ratio was set at 15%. These details are more succinctly listed below in Table 3, and the results are shown in Fig. 10(a) and (b).

The highest level of fluoride ion released in effluent in the first result can be found at the first point of the constant aging, suggesting that the chemical degradation during non-operation influences the fluoride release. From the fact that the lowest concentration of fluoride ion in the Fig. 10(b) is at the first point of the dynamic operation, it is thought to be that the degradation occurred during overnight cessation can be neglected by the constant aging for 2.5 h. And also, the fluoride emission increased and saturated over about 8 h during the dynamic operation.

The frequency effect on chemical degradation is plotted in Fig. 11. Fluoride emission increases up to peak around 0.1 Hz and then decreases with further frequency increases. In examining the data in Fig. 11(a), it appears that the fluoride emission is relatively constant for frequencies above 20 Hz. If it is assumed that the emissions at 1 kHz are essentially the same as for constant-current operation, then the difference in fluoride emissions between the constant and dynamic operations would appear to be on the order of two, rather than the variation of a factor of 10 reported by Liu and Case [8]. This could be from different experimental conditions in which the cyclic operation condition included open circuit [8].

It is interesting to compare the frequency dependence of the fluoride emission with the voltage response of the first *RC* cell (R_1 and C_1) listed in Table 2. The two sets of data are both shown in Fig. 11(b). In that figure, the frequency range can be divided by three zones: a full oscillation region (DC–0.2 Hz), a transition region (0.2–10 Hz), and no oscillation region (>10 Hz). The fluoride emissions increase with frequency across the full oscillation region, then decrease across the transition region and finally become indepen-

Table 2
Frequency ranges of the input signal leading to the voltage oscillation.

	R_{ct}	R_1 and C_1	R_2 and C_2
Full oscillation range	DC–20 Hz	DC–0.2 Hz	DC–2 Hz
Decreasing amplitude range	>100 Hz	0.2–10 Hz	10 Hz–over 100 Hz
No oscillation range	–	10 Hz–higher frequency	–

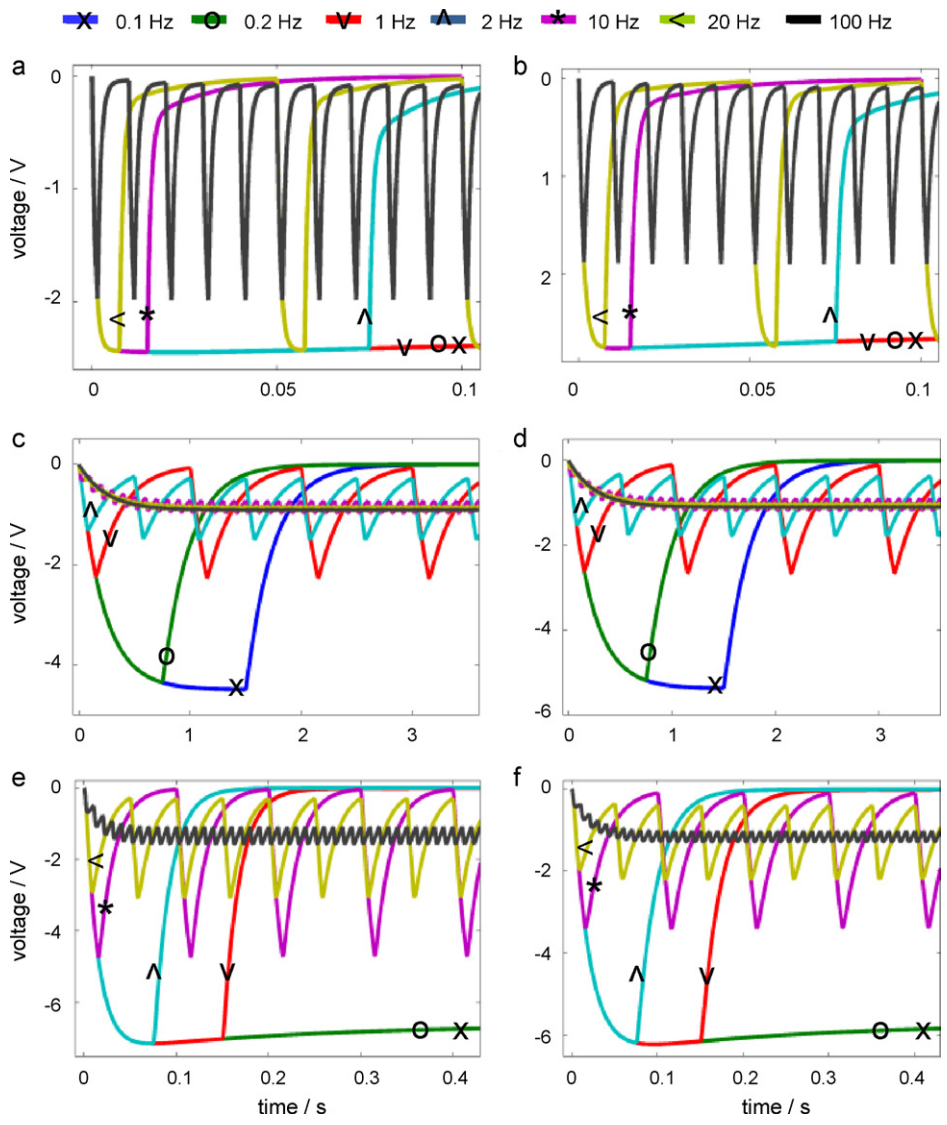

Fig. 9. Voltage response dropped by R_{ct} simulated using the parameters from (a) the down curve and (b) the up curve. (c) and (d) are from the down and the up curves by the first *RC* cell (R_1 and C_1), and (e) and (f) by the second *RC* cell (R_2 and C_2).

Table 3
Experimental order and condition for dynamic operation of the Nexa system.

Day	Freq. of input signal	Duty ratio	Cessation period	Constant Current aging	Time for sampling the effluent
1	1 kHz	15%	~1 month	4.5 h	2 h, 4 h, 5.5 h, 7 h
2	0.1 Hz	15%	Overnight	2.5 h	2 h, 4 h, 5.5 h, 7 h, 8.5 h, 10 h, 11.5 h
3	0.0005 Hz	15%	Overnight	2.5 h	2 h, 4 h, 5.5 h, 7 h
4	1 Hz	15%	Overnight	2.5 h	2 h, 4 h, 5.5 h, 7 h
5	20 Hz	15%	Overnight	2.5 h	2 h, 4 h, 5.5 h, 7 h
6	0.001 Hz	15%	Overnight	2.5 h	2 h, 4 h, 5.5 h, 7 h
7	5 Hz	15%	Overnight	2.5 h	2 h, 4 h, 5.5 h, 7 h
8	0.01 Hz	15%	Overnight	2.5 h	2 h, 4 h, 5.5 h, 7 h

dent of frequency in the no oscillation region. As mentioned in the previous discussion of modeling, the first RC cell represents the time delay corresponding to water transport in the membrane [11,12]. It is thus supposed that the accelerated degradation of the membrane (as indicated by the increased fluoride emissions) is closely related to water transport inside the membrane.

4. Discussion

The result of Fig. 11 showed that the periodic water transport inside the membrane plays an important role in the chemical degradation. In general, water transport in the membrane is considered as to result in dehydration and hydration at the anode and cathode sides of the membrane respectively because of electro-osmotic drag [13]. There are four kinds of water movement occurring inside the membrane, electro-osmotic drag, back diffusion, evaporation into air at the cathode, and supply from external humidifier at the cathode and/or the anode [13]. In case of the Ballard Nexa system having very thin membrane (3.5×10^{-5} m) and just one side humidifier at the cathode [14], the back diffusion of the water may play a serious role in the water movement [13,15]. The anode side of the membrane usually experiences the humidity cycle, but

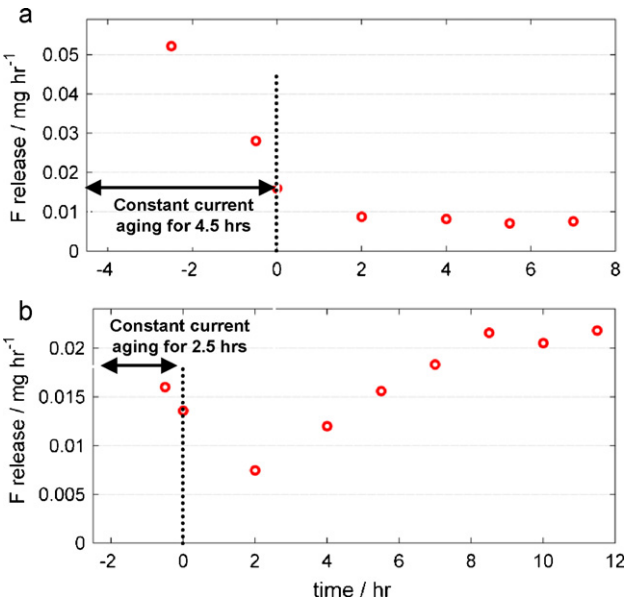

Fig. 10. Fluoride release during the operation (a) at 1 kHz and (b) at 0.1 Hz.

the cathode side is fully saturated with water at all times. There are reports indicating that humidity cycles may induce mechanical stresses [16,17]. Moreover, it was shown that membrane thinning and pin-holes generation were accelerated in the area corresponding to the stress concentration points [18]. Therefore, one possible reason for accelerated degradation of dynamic operation is the periodic stress induced by the humidity cycles even though the stress is not enough to cause mechanical deformation.

Another possible reason suggested in this paper is related to diffusion of H_2O_2. Electro-osmotic drag of water is the mass flux caused by a polarity of the water molecules attracted to the positively charged protons moving from the anode to the cathode [19]. Since H_2O_2 has dipole moment of 2.2 Debye which is bigger than water (1.85 Debye), it can be also dragged by the moving protons and periodically transported by the cyclic operation in the same fashion as the water. H_2O_2 is generated at the anodic catalyst layer

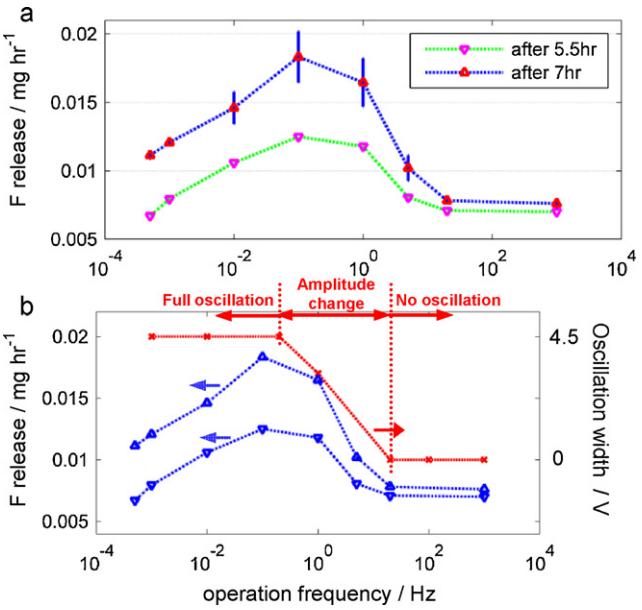

Fig. 11. (a) Fluoride release during dynamic operation in terms of frequency variation and (b) relationship between the voltage oscillation of the first *RC* cell and fluoride emission in terms of the frequency change.

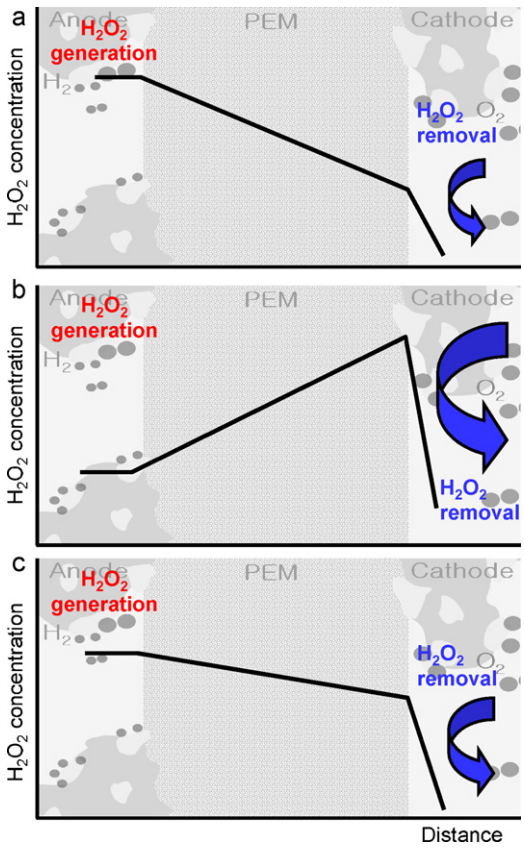

Fig. 12. Concentration of H_2O_2 inside the membrane during operation (a) at open circuit, (b) during switch on (large current), and (c) during switch off (small current).

by the direct combustion of hydrogen with crossover oxygen or incomplete reduction of oxygen on the Pt surface [1,6]. Furthermore, contaminants such as chloride ions and carbon monoxide can increase the yield of H_2O_2 drastically [1]. Such H_2O_2 formation reactions can also occur at the cathode catalyst layer [1,20]. However, H_2O_2 is so reactive to be decomposed into water relatively quickly on the Pt surface [20], and it can be assumed that there is a little chance for H_2O_2 to be accumulated on the Pt surface before it diffuses into the membrane. This assumption can be applied to just the cathode catalyst layer because a monolayer of hydrogen on the Pt surface at the anode inhibits the decomposition of H_2O_2. For this reason, it is widely believed that H_2O_2 formation occurs mainly at the anodic catalyst layer [1,21]. With no current, H_2O_2 formed at the anode would diffuse into the cathode and be removed by decomposition on the Pt surface or evaporation into the air. The concentration of H_2O_2 at the anode and the cathode sides of the membrane would depend on the yield of H_2O_2 at the anode and the removal rate of H_2O_2 at the cathode, which is described in Fig. 12(a). Even small currents could reduce the H_2O_2 concentration at the anode side of the membrane due to the electro-osmotic drag, and the total amount of H_2O_2 inside the membrane would decrease because the accumulation of H_2O_2 at the cathode could expedite the removal rate as shown in Fig. 12(b) (a bigger arrow), which can explain the accelerated degradation at open circuit condition. As the current stops or decreases during the dynamic operation condition, redistribution of H_2O_2 may occur inside the membrane due to the back diffusion under the circumstance of accumulated H_2O_2 at the cathode side and H_2O_2 generation at the anode layer, which could explain deteriorated degradation during dynamic operation. In addition, the serious effect of the low humidification on the degradation mentioned in the introduction can be explained by the higher dipole moment of H_2O_2 than that of the

water. It was reported through simulation research [22] that most water molecules are constrained by sulfonate heads in the membrane at low water contents. H_2O_2 would also be constrained by them, besides, more strongly than water due to its larger polarity, so most H_2O_2 could make contributions in formation of reactive oxygen radicals with little chance to diffuse out to the cathode.

5. Conclusions

The frequency effect of the dynamic operation on the chemical degradation was investigated in this research. Firstly, the Ballard Nexa system was analyzed by a modified Randles model and curve fitting, and dynamic behavior of it as the change of frequency was simulated using MATLAB Simulink®. Secondly, the fluoride release in terms of the frequency change was evaluated by measuring the concentration of fluoride ion in the drain water of the Nexa system. The comparison between above two results showed that accelerating factor of the dynamic operation on the chemical degradation is closely related to water transport inside the membrane. Two possibilities of the accelerating factor were presented. One is the stress induced by cyclic humidity, as suggested by other sources and the other is periodic transport of H_2O_2 inside the membrane.

Appendix A. Supplementary data

Supplementary data associated with this article can be found, in the online version, at doi:10.1016/j.jpowsour.2010.10.105.

References

[1] A. Collier, H. Wang, X.Z. Yuan, J. Zhang, D.P. Wilkinson, International Journal of Hydrogen Energy 31 (2006) 1838–1854.
[2] M. Inaba, T. Kinumoto, M. Kiriake, R. Umebayashi, A. Tasaka, Z. Ogumi, Electrochimica Acta 51 (2006) 5746–5753.
[3] A.B. LaConti, M. Hamdan, R.C. McDonald, in: W. Vielstich, H.A. Gasteiger, A. Lamm (Eds.), Handbook of Fuel Cells, vol. 3, John Wiley & Sons, New York, 2003, pp. 648–662.
[4] J. Healy, C. Hayden, T. Xie, K. Olson, R. Waldo, M. Brundage, H. Gasteiger, J. Abbott, Fuel Cells 5 (2005) 302–308.
[5] J. Yu, T. Matsuura, Y. Yoshikawa, M.N. Islam, M. Hori, Solid-State Letters 8 (2005) A156–A158.
[6] M. Inaba, H. Yamada, R. Umebayashi, N. Sugishita, A. Tasaka, Membrane degradation in polymer electrolyte fuel cells under the low humidification conditions, The Electrochemical Society of Japan 75 (2007) 207–212.
[7] A. Ohma, S. Suga, S. Yamamoto, K. Shinohara, Journal of the Electrochemical Society 154 (2007) B757–B760.
[8] D. Liu, S. Case, Journal of Power Sources 162 (2006) 521–531.
[9] Nexa™ Power Module User's Manual, Ballard Power Systems, Inc. Document No. MAN5100078 (2003).
[10] Fluoride Selective Ion Electrode (Model No. 51928) Instruction Manual, Hach Inc., http://www.hach.com/fmmimghach?/CODE:51928884391.
[11] M. Jung, M.D. Ashford, K.A. Williams, Analysis of a fuel cell system by a step response, Fuel Cells, in press, doi:10.1002/fuce.201000007.
[12] M. Bautista, Y. Bultel, P. Ozil, 4th International Conference on Electrocatalysis (ECS'02), PD03 (Poster), 2002.
[13] J. Laminie, A. Dicks, Fuel Cell Systems Explained, 2nd ed., Wiley, 2003.
[14] A.J. del Real, A. Arce, C. Bordons, Journal of Power Sources 173 (2007) 310–324.
[15] S. Um, C.-Y. Wang, Journal of Power Sources 156 (2006) 211–223.
[16] H. Tang, S. Peikang, S.P. Jiang, F. Wang, M. Pan, Journal of Power Sources 170 (2007) 85–92.
[17] A. Kusoglu, A.M. Karlsson, M.H. Santare, S. Cleghorn, W.B. Johnson, Journal of Power Sources 170 (2007) 345–358.
[18] V. Stanic, M. Hoberecht, Electrochemical Society Proceedings 21 (2004) 391–401.
[19] M.M. Mench, Fuel Cell Engines, John Wiley and Sons, 2008, p. 312.
[20] V.O. Mittal, H.R. Kunz, J.M. Fenton, Electrochemical and Solid-State Letters 9 (2006) A299–A302.
[21] U.A. Paulus, T.J. Schmidt, H.A. Gasteiger, R.J. Behm, Journal of Electroanalytical Chemistry 495 (2001) 134–145.
[22] J. Fimrite, H. Struchtrup, N. Djilali, Journal of the Electrochemical Society 152 (2005) A1804–A1814.